Mesozoic 001 (2): 192–207
https://www.mapress.com/mz/

Article

ISSN 3021-1859 (print edition)
MESOZOIC
ISSN 3021-1867 (online edition)

https://doi.org/10.11646/mesozoic.1.2.11
http://zoobank.org/urn:lsid:zoobank.org:pub:51BD5F78-1DCD-4FD5-8874-A1AB134236ED

Discussion on the age of the Early Cretaceous amber from the Hailar Basin, NE China

HAI-LONG GAO[1], YI-TONG SU[2], CHEN-YANG CAI[2], DANY AZAR[2], XIANG-BO SONG[2], XIN-NENG LIAN[1] & DI-YING HUANG[2,*]

[1]*School of Earth Sciences, East China University of Technology, Nanchang, Jiangxi 330013, China*
[2]*State Key Laboratory of Palaeobiology and Stratigraphy, Nanjing Institute of Geology and Palaeontology, Chinese Academy of Sciences, Nanjing 210008, China*

cugloong@163.com; https://orcid.org/0000-0002-6365-9983
ytsu@nigpas.ac.cn; https://orcid.org/0000-0003-0547-0792
cycai@nigpas.ac.cn; https://orcid.org/0000-0002-9283-8323
danyazar@ul.edu.lb; https://orcid.org/0000-0002-4485-197X
xbsong@nigpas.ac.cn; https://orcid.org/0009-0009-7153-1005
lianxinneng@stu.ynu.edu.cn; https://orcid.org/0000-0001-6680-1781
dyhuang@nigpas.ac.cn; https://orcid.org/0000-0002-5637-4867
**Corresponding author*

Abstract

Amber in China is predominantly found from the Cenozoic era, with the oldest-known amber originating from the Middle Triassic Qingyan biota in Guiyang, Guizhou. Chinese Cretaceous amber has been known from Xixia and Neixiang (Henan Province), Guangzhou (Guangdong Province), and the Buir Lake area (Inner Mongolia). Some previous studies have suggested that the amber found at the base of the Yimin Formation in the Yimin Coal Mine in the Hailar Basin (130.9 ± 2.8 Ma, as constrained by detrital zircon U-Pb dating in the original paper) represents the oldest known amber in China at that time. In this paper, detrital zircon U-Pb dating was conducted on the clastic rocks from the Damoguaihe Formation of the Zhalainuoer Coal Mine, Hailar Basin to contest the age of the Buir Lake amber. Our results suggest that the upper part of the Damoguaihe Formation was deposited earlier than 116 Ma (late Aptian), consistent with biostratigraphy and isotopic chronology. Therefore, the age of the amber-bearing Damoguaihe Formation in Hailar Basin should be slightly older than 116 Ma. Amber from the Yimin Formation was discovered from two layers, with the lower layer (the first coal seam) likely near the Aptian–Albian boundary and the upper layer slightly later than 111.7 Ma. Our analyses further confirm that Buir Lake ambers are from the upper Lower Cretaceous Damoguaihe Formation and Yimin Formation, dating to the Aptian–Albian.

Keywords: amber, Damoguaihe Formation, Yimin Formation, U-Pb geochronology

Introduction

Amber is a fossilized tree resin found worldwide, which has important aesthetic and scientific value (Stilwell *et al*., 2020; Roghi *et al*., 2022; Delclòs *et al*., 2023). The oldest known amber in the world was found in the Pennsylvanian strata of Illinois, U.S.A. (Bray & Anderson, 2009). Amber discovered from the pre-Cenozoic strata in China are very limited: the oldest known amber was reported from the Anisian Stage of the Middle Triassic Qingyan biota in Guiyang (Tian *et al*., 2024); Tiny Jurassic amber piece has been discovered in the Middle–Late Jurassic Daohugou biota, although it has not yet been formally reported; Early Cretaceous amber has been reported from the Damoguaihe Formation at the Zhalainuoer Coal Mine, Manzhouli, Inner Mongolia (Fig. 1), though it comprised a tiny specimen (Azar *et al*., 2019); Late Cretaceous amber has been abundantly discovered in the Shigou Formation of the Upper Cretaceous in Xixia County, Nanyang City, Henan Province (Shi *et al*., 2014), and has also been found in the Dalangshan Formation of the Upper Cretaceous in Guangzhou (Ni *et al*., 2023).

Li *et al*. (2023) discovered amber in the Yimin Formation coal seams of the Zhalainuoer and Yimin coal mines in the Hailar Basin, with both ambers being fossilized in gymnosperm leaves of consistent morphology. Zircon U-Pb isotopic dating provided absolute ages of 111.7 ± 2.2 Ma and 130.9 ± 2.8 Ma, respectively, to constrain the lower age limit of the amber. The stratigraphic positions

 Submitted: 22 Jun. 2024; accepted by Z. Feng: 26 Jun. 2024; published: 27 Jun. 2024

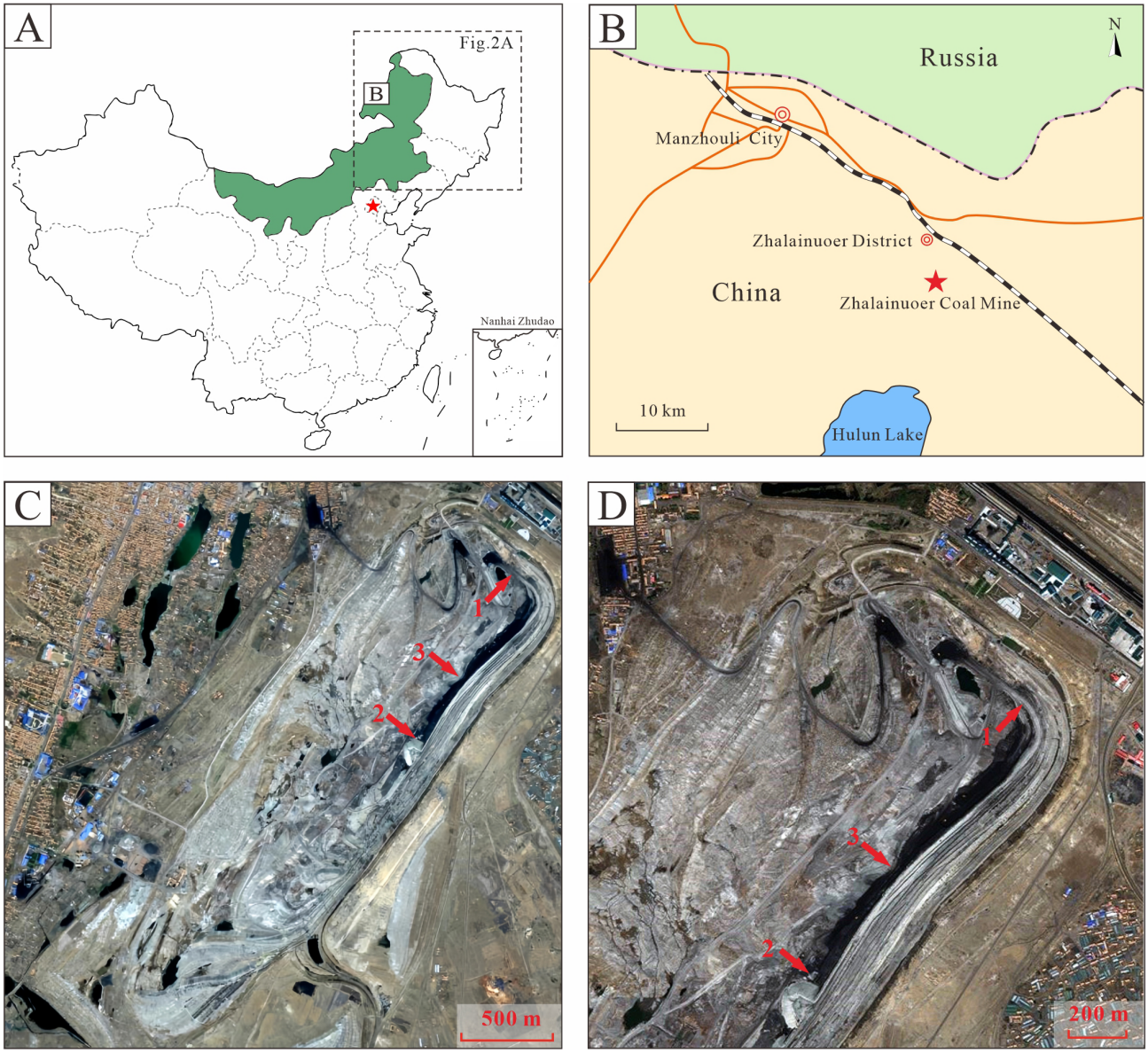

FIGURE 1. Map of amber locality. **A**, Map of China showing locality of Zhalainuoer. Inner Mongolia, China. **B**, Detailed locality of Zhalainuoer Coal Mine, after Azar *et al*., 2019. **C**, **D**, Aerial photography of Zhalainuoer Coal Mine. Arrows show locality where the amber was found. Arrow 1, amber layer in Damoguaihe Formation (Azar *et al*., 2019). Arrow 2, locality of amber layer in Yimin Formation by Li *et al*., 2023. Arrow 3, locality of amber-bearing layer in this study.

of the amber show a good correlation, suggesting that the age of the Yimin Formation coal seam where amber was found is likely very close to 111.7 ± 2.2 Ma, representing an early Albian age, while the absolute age of 130.9 ± 2.8 Ma from the Yimin Coal Mine likely represents inherited zircon without specific chronological significance. Therefore, multiple amber-bearing layers are present in the Zhalainuoer Coal Mine, including the Damoguaihe Formation below the coal seam (Azar *et al*., 2019) and different levels of the Yimin Formation (Li *et al*., 2023). Cretaceous amber from the Buir Lake region has long been reported (Zhong, 2003) that supposed to be the earliest Chinese amber with *ca*. 130 Ma old, but its exact age and stratigraphic correlation have not been clearly studied.

In this study, we present detrital zircon U-Pb age analyses for the clastic rocks from the upper part of the Damoguaihe Formation and contest the ages of the amber-bearing layers in the Hailar Basin.

Geological setting and sampling

Geological setting

NE China (Fig. 1A, B) is located in the eastern part of the Central Asian Orogenic Belt, which was formed by accretion of island arcs, ophiolites, oceanic islands, seamounts, accretionary wedges, oceanic plateaus and

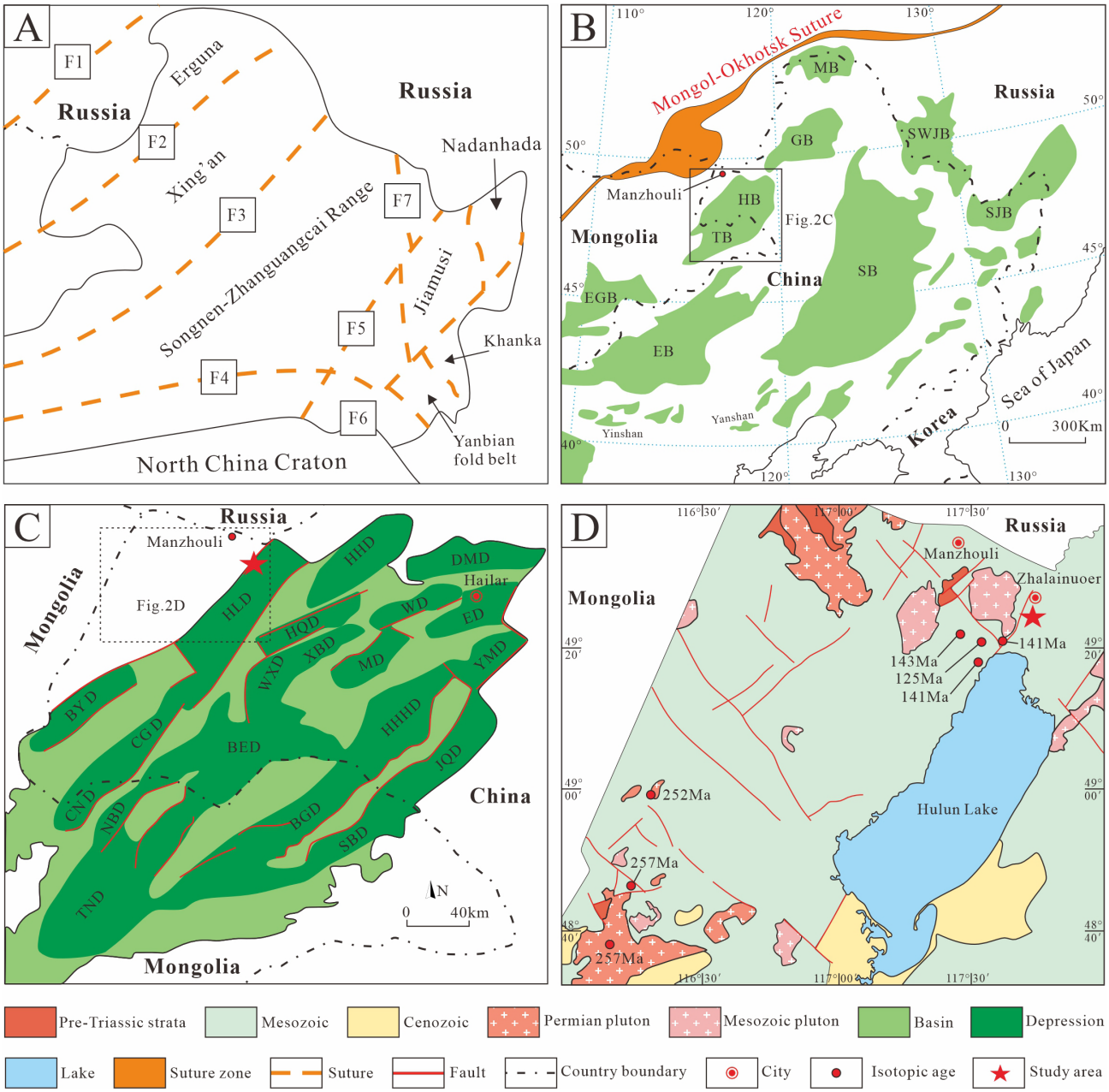

FIGURE 2. Simplified tectonic and geological maps of study area. **A**, Tectonic subdivisions of NE China (modified after Xu *et al*., 2013). F1: Mongol-Okhotsk Belt; F2: Tayuan-Xiguitu Fault; F3: Hegenshan-Heihe Fault; F4: Solonker-Xra Moron Fault; F5: Yitong-Yilan Fautl; F6: Dunhua-Mishan Fault; F7: Mudanjiang Fault. **B**, Mesozoic basins in NE China (modified after Ji *et al*., 2019). **C**, Depressions in Hailar Basin (modified after Ji *et al*., 2019). Abbreviations: EB, Erlian Basin; EGB, East Gobi Basin; HB, Hailar Basin; TB, Tamsag Basin; SB, Songliao Basin; GB, Genhe Basin; MB, Mohe Basin; SWJB, Sunwu-Jiayin Basin; SJB, Sanjiang Basin. **D**, Simplified geological map of Zhalainuoer Coal Mine (modified after Gou *et al*., 2013; Meng *et al*., 2011).

microcontinents (Şengör *et al*., 1993; Windley *et al*., 2007). Following the closure of the Paleo-Asian Ocean in the Palaeozoic, multiple microcontinental massifs amalgamated (Wilde & Zhou, 2015), including the Erguna, Xing'an, Songnen-Zhangguangcai Range, Jiamusi, and Khanka massifs from the west to east (Fig. 2A; Xu *et al*., 2013). These massifs were separated by several sutures, as illustrated in Fig. 2A. During the late Mesozoic, NE China experienced an extensional environment due to the combined influences of Paleo-Pacific and Mongol-Okhotsk domains (Xu *et al*., 2013), leading to widespread magmatism and a series of basins with volcanic-sedimentary strata, such as Erlian, Songliao, Genhe, Mohe, and Hailar-Tamstag basins (Fig. 2B).

The Hailar Basin is located in the westernmost region of NE China and straddles the Erguna and Xing'an blocks (Fig. 2B). It extends into NE Mongolia as the Tamtsag Basin (Fig. 2B; Ji *et al*., 2019). The Hailar Basin consists

of a series of depressions that formed synchronously under an extensional tectonic regime (Fig. 2C), and our study area is located in the western part of the Hulunhu Depression (Fig. 2C, D). Previous studies have pointed out that the Erguna Block is composed of Paleoproterozoic metamorphic basement, Neoproterozoic granitoids, voluminous Paleozoic and Mesozoic granitoids and Mesozoic volcanic rocks (Xu *et al*., 2013). The Xing'an block consists mainly of abundant Mesozoic granitoids, volcanic rocks, and Palaeozoic metamorphic rocks (Xu *et al*., 2013).

The stratigraphic succession in Hailar Basin could be divided into four groups: the pre-Jurassic Budate Group, Upper Jurassic–Lower Cretaceous Xing'anling, Zalainuoer and Beierhu groups in ascending order (Wan, 2006; A *et al*., 2013). The Budate Group, considered as the uppermost part of the basement, consists of conglomerates, sandstones, interlayered volcanics and low-grade metamorphic rocks. This unit has been dated to be Carboniferous–early Permian by zircon U-Pb dating (Meng *et al*., 2013). Some scholars considered that a series of Triassic volcanic rocks overlie the Budate Group because related isotopic ages (*ca*. 214 Ma) have been reported (Chen *et al*., 2016).

The Late Jurassic–Early Cretaceous Xing'anling Group is a syn-rift succession, comprising the Tamulangou, Tongbomiao, and Nantun formations in ascending order. The Late Jurassic Tamulangou Formation is characterized by basic-intermediate volcanic rocks and sedimentary layers. Spore-pollen assemblages in the Tamulangou Formation show the biostratigraphic features from the late Middle Jurassic to Late Jurassic period, consisting with the zircon U-Pb dating of the volcanic rocks aged from 157 to 148 Ma (Li *et al*., 2010; Chen *et al*., 2016; Ji *et al*., 2019). The predominant Tongbomiao and Nantun formations consist of interlayered conglomerates, sandstones, siltstones and mudstones deposited in alluvial and lacustrine environments, occasionally interbedded with minor volcanic rocks (Wan, 2006). The volcanic layers in the Tongbomiao Formation yielded age constraints ranging from 142 to 137 Ma (Ji *et al*., 2019), corresponding to the Berriasian–early Valanginian period, which is consistent with the findings of palynological studies (Wan, 2006). The Lower and Upper members of the Nantun Formation are reassigned to *ca*. 131–120 Ma and *ca*. 117–111 Ma, respectively (Ji *et al*., 2019). Based on the presence of a spore-pollen assemblage of *Foraminisporis asymmetricus—Classopollis* sp.—*Pseudopicea* sp., the age of the Nantun Formation has been determined to be Valanginian (Table 1; Wan, 2006). The geological age of this unit was constrained as 138–127 Ma (Zhao *et al*., 2015) or 131–111 Ma (Ji *et al*., 2019). Although there is ongoing debate regarding the division and correlation scheme of the Xing'anling Group, it is generally considered as a set of volcanic-sedimentary strata with several concentrated volcanic eruptions.

The fluvial-delta and lacustrine phase Zhalainuoer Group, bounded by thick mudstones, could be divided into the Damoguaihe and Yimin formations. Both are coal-bearing strata, with the Yimin Formation exhibiting a greater abundance of thicker coal layers. The Damoguaihe Formation was assigned to be Valanginian–Barremian (Table 1; Pu & Hong, 1985; Meng *et al*., 2003; Wan, 2006; Li *et al*., 2007; Xue & Wang, 2010; Wang *et al*., 2014) based on the presence of a spore-pollen assemblage consisting of *Cicatricosisporites australiensis-Motonisporites equiexinus-Protopicea* sp.. While the ostracod assemblage of *Cypridea (Cypridea)—Cypridea (Ulwellia)—Limnocypridea* suggests a Barremian–Aptian age (Table 1; Wang *et al*., 2012). The Yimin Formation was assigned to be Barremian–Aptian due to the occurrence of *Appendicisporites—Impardecipora—Triporoletes* (Table 1; Pu & Wu, 1985; Wan, 2006; Xue, 2017). Additionally, the Zhalainuoer Group has been suggested to be Barremian–Albian as the co-occurrence of algae assemblage of *Nyktericysta* and *Vesperopsis* (Wu *et al*., 2006). The identification of angiosperm pollen in the Damoguaihe Formation, such as *Asteropollis, Tricolpites* and *Polyporites*, indicates that this formation may be younger than previously considered, possibly Barremian–early Albian (Table 1; Huang *et al*., 2006). Some authors propose an Aptian–Albian age for the underlying Nantun Formation (Han *et al*., 2019; Ji *et al*., 2019), implying that the Zhalainuoer Group is younger than Albian.

The uppermost Beierhu Group comprises the Late Cretaceous Qingyuangang and the Paleocene Huchashan formations, consisting of alluvial and fluvial conglomerates and mudstones (Wan, 2006).

Material and methods

New amber material

In the lower part of the Yimin Formation (Fig. 3), more than ten small amber grains (Fig. 4) were obtained from the first layer of coal. The photographs of the amber grains were taken using a digital camera attached to a Zeiss Discovery V20 microscope and a Canon 5D Mark II camera with a 100 mm macro lens. The specimens are housed in the Nanjing Institute of Geology and Palaeontology, Nanjing, China.

These amber grains exhibit a golden yellow colour and are relatively transparent, with a particle size generally not exceeding 1 mm. They are typically lump-shaped, with some taking on the form of pancakes (Fig. 4). Under ultraviolet light, the amber fluoresces a light yellow. The output beds of these amber particles are significantly

TABLE 1. Summary of chronological constraints on amber-bearing strata yielded by fossils in Hailar Basin, NE China.

Formation	Geological age	Fossil assemblages		Reference
Yimin Formation	Barremian–Aptian	spore-pollen assemblage	*Appendicisporites-Impardecipora-Triporoletes*	Pu & Hong, 1985; Wan, 2006; Xue, 2017
	Barremian–Albian	algae assemblage	*Nyktericysta* and *Vesperopsis*	Wu *et al*., 2006
Damoguaihe Formation	Valanginian-Barremian	spore-pollen assemblage	*Cicatricosisporites australiensis-Motonisporites equiexinus-Protopicea sp.*	Pu & Hong, 1985; Meng *et al*., 2003; Wan, 2006; Xue & Wang, 2010; Wang *et al*., 2014
	Barremian–Aptian	ostracod assemblage	*Cypridea (Cypridea)-Cypridea (Ulwellia)-Limnocypridea*	Wang *et al*., 2012
	Barremian–early Albian	angiosperm pollen	*Asteropollis, Tricolpites* and *Polyporites*	Huang *et al*., 2006
Nantun Formation	Aptian–Albian	spore-pollen assemblage	upper part: *Concentrisporites-Piceaepollenites-Pinuspollenites*	Han *et al*., 2019
			lower part: *Piceaepollenites-Pinuspollenites-Abietineaepollenites;*	Han *et al*., 2019
	Valanginian	spore-pollen assemblage	*Foraminisporis asymmetricus-Classopollis sp.-Pseudopicea sp.*	Wan, 2006

FIGURE 3. Stratigraphic column of Zhalainuoer Group and field photos in Zhalainuoer Coal Mine. **A**, Amber-bearing coal layer in Yimin Formation. **B**–**D**, Sampling locations of the sample NMGZLN007, NMGZLN006, and NMGZLN004, respectively.

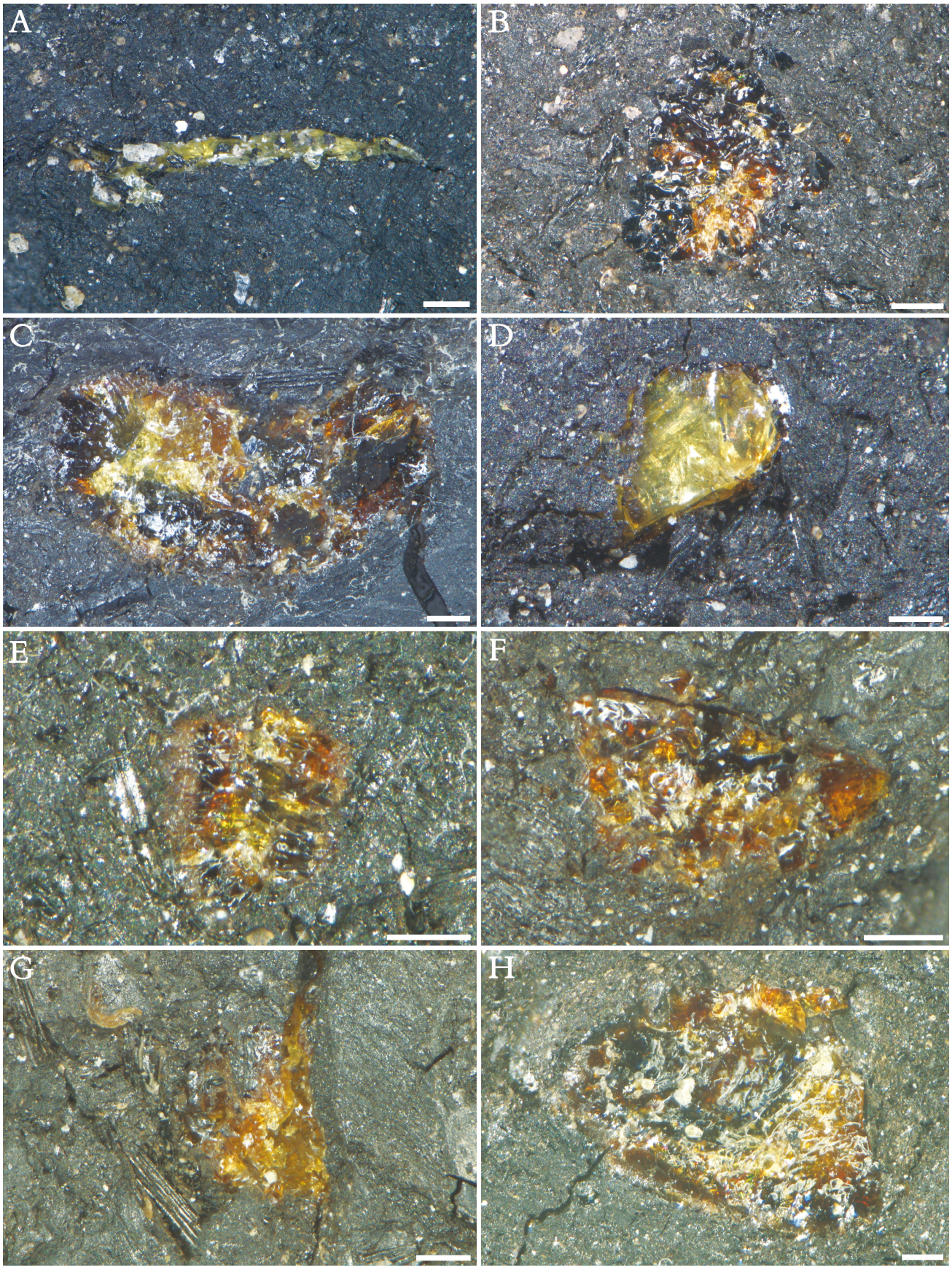

FIGURE 4. Micrographs of amber from Zhalainuoer Coal Mine, Hailar Basin. scale bars = 200 μm.

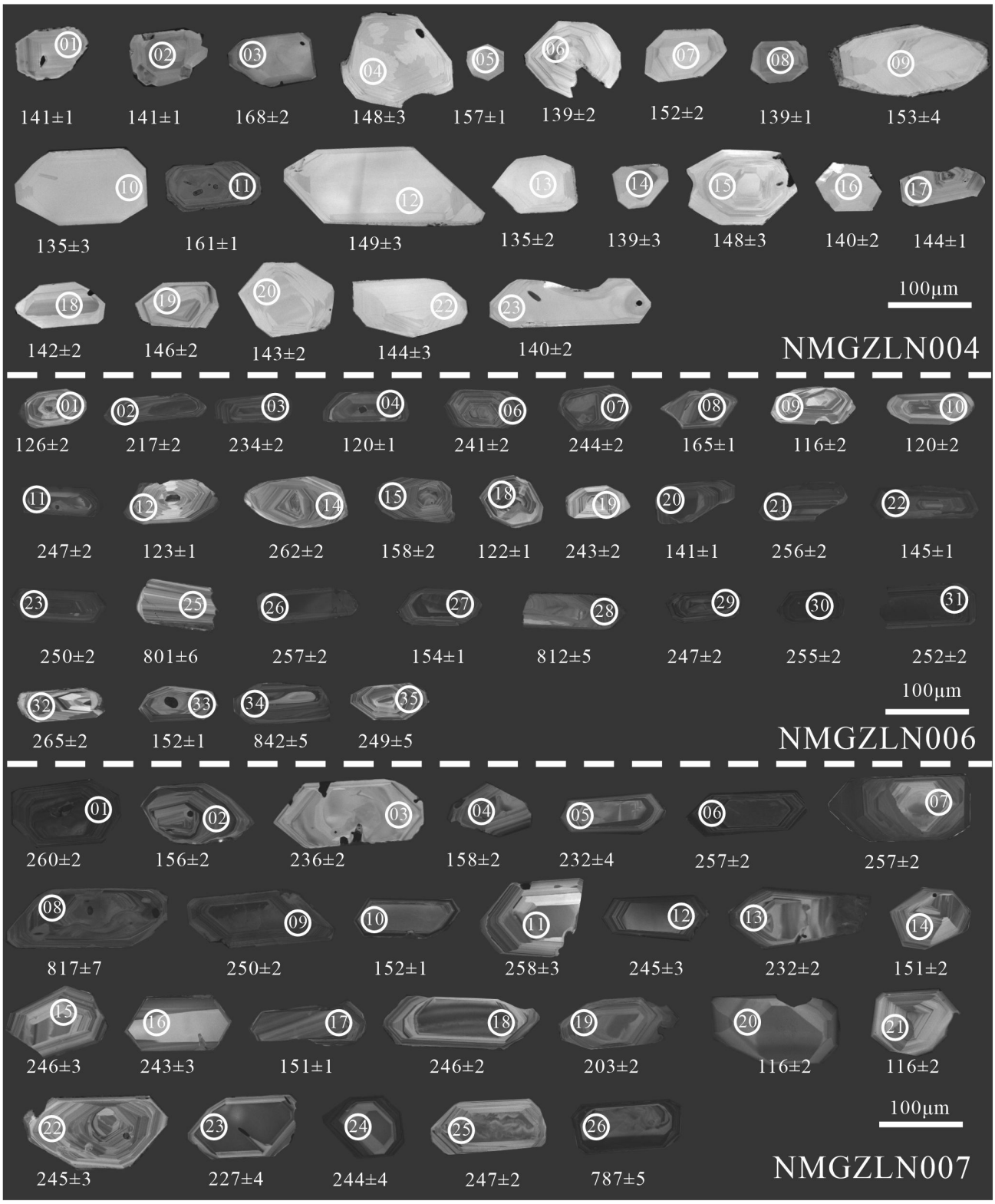

FIGURE 5. CL images of representative zircons from three samples of Damoguaihe Formation in Hailar Basin, Zhalainuoer, Inner Mongolia. White circles show locations of analysis spots, and U-Pb ages (Ma) are provided nearby.

higher than those reported by Azar *et al*. (2019) in the upper part of the Damoguaihe Formation in Zhalainuoer Coal Mine, and they belong to the same coal seam as the amber from the Yimin Formation in Zhalainuoer Coal Mine as reported by Li *et al*. 2023.

Zircon U-Pb dating

Three clastic rock samples (NMGZLN004, NMGZLN006, and NMGZLN007) were collected from the Damoguaihe Formation (Fig. 3). The samples NMGZLN004 and

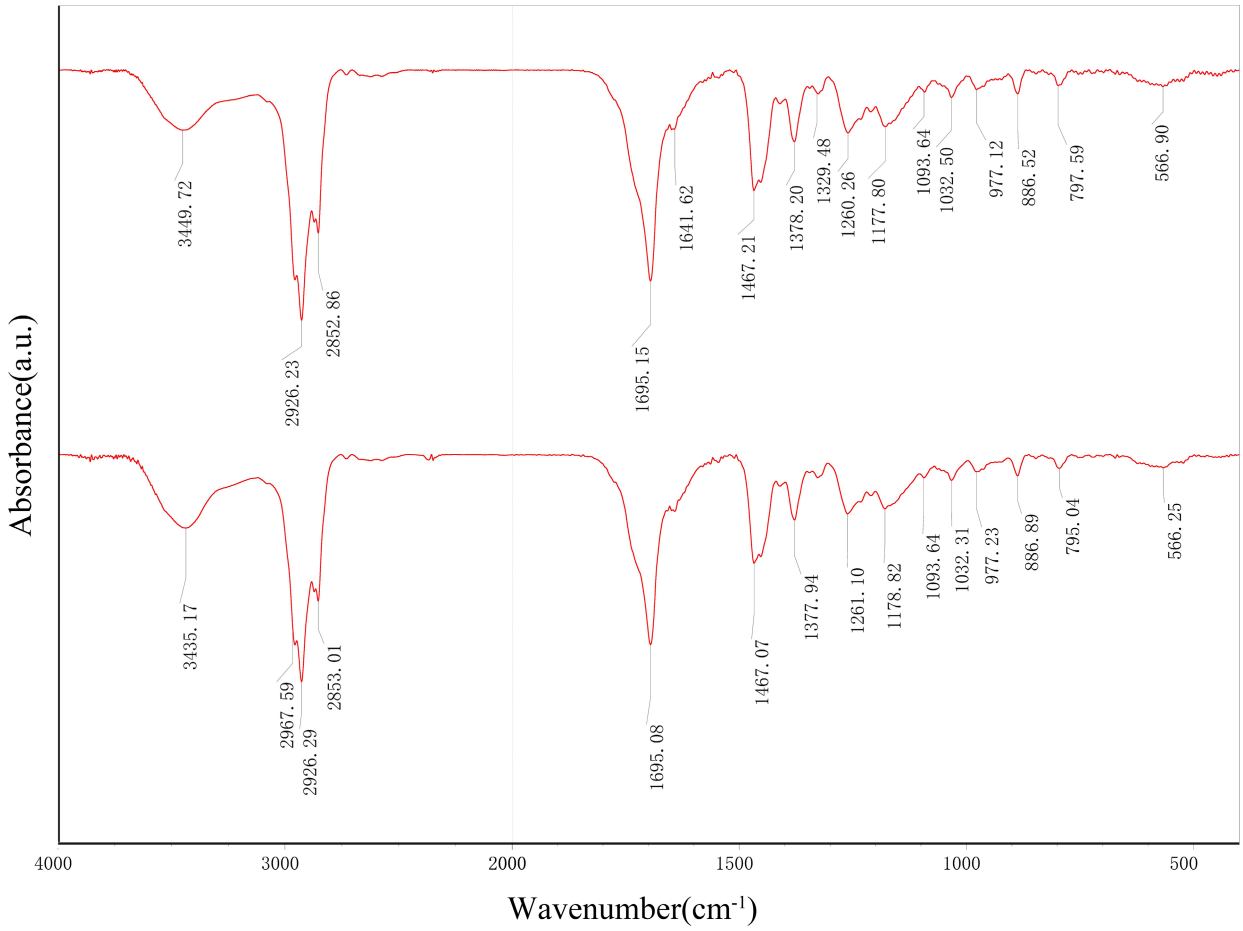

FIGURE 6. FTIR spectra of two amber samples from Zhalainuoer Coal Mine, Hailar Basin. **A**, Analyzed by method 1. **B**, Analyzed by method 2.

NMGZLN006 are situated below the amber-bearing layer of the Damoguaihe Formation.

The zircon grains were separated using conventional magnetic and heavy liquid techniques and hand-picking under a binocular microscope. The selected zircon grains were embedded in epoxy resin, polished, and gold-coated for analysis. Images of the grains were captured under transmitted and reflected light, along with cathodoluminescence (CL) imaging (Fig. 5), to aid in identifying suitable spots for in situ analysis. The zircon U-Pb isotopic analyses were performed using an Agilent 7500 LA-ICP-MS instrument at the State Key Laboratory of Continental Dynamics, Northwest University, Xi'an, China. The off-line selection and integration of background and signals, time-drift correction and quantitative calibration were conducted using GLITTER 4.0 software. Zircon U-Pb concordia and weighted mean age plots were produced using Isoplot/Ex_ver3.0 (Ludwig, 2003). The analytical results are listed in Table 2.

FT-IR analysis

For the infrared analysis, the amber was analyzed following two methods: 1) 0.2 mg of amber was crushed and mixed with potassium bromide (KBr) and pellets were prepared using a hydraulic manual press, in this case, the spectrum was acquired between 4000 and 400 cm^{-1} with 40 scans collected at 4 cm^{-1} resolution (Fig. 6A); and 2) directly and the spectrum was acquired between 4000 and 400 cm^{-1} (Fig. 6B). Transmission FT-IR spectroscopy was performed with a Bruker VERTEX and HYPERION 2000 spectrophotometers.

Results

Zircon U-Pb dating

The zircon grains extracted from the clastic rocks exhibit a colourless and euhedral appearance, measuring approximately 50–300 μm in size, with length-to-width ratios spanning from 1:1 to 6:1. Most of the grains exhibit well-developed oscillatory zoning in CL images (Fig. 5). Analyses of the zircons reveal a wide range of Th (44–1304 ppm) and U (48–831 ppm) concentrations, with Th-U ratios range from 0.3 to 1.9, indicative of an igneous

TABLE 2. Results of LA-ICP-MS zircon U-Pb analyses for clastic rocks from Damoguaihe Formation in Zhalainuoer Coal Mine, Zhalainuoer, Inner Mongolia, NE China.

Analyses					$^{207}Pb/^{206}Pb$		$^{207}Pb/^{235}U$		$^{206}Pb/^{238}U$		$^{207}Pb/^{206}Pb$		$^{207}Pb/^{235}U$		$^{206}Pb/^{238}U$		
	Pb	Th	U	Th/U	Ratio	1σ	Ratio	1σ	Ratio	1σ	Age	1σ	Age	1σ	Age	1σ	concordance
NMGZLN004																	
01	29	1304	699	1.9	0.04881	0.00122	0.1483	0.00342	0.02203	0.00016	138.6	57.8	140.4	3.0	140.5	1.0	99.9
02	19	504	608	0.8	0.04894	0.00122	0.1494	0.00343	0.02214	0.00016	145.2	57.4	141.4	3.0	141.1	1.0	99.8
03	11	196	321	0.6	0.04958	0.00192	0.18018	0.00668	0.02635	0.00026	175.5	88.1	168.2	5.8	167.7	1.7	99.7
04	2	83	65	1.3	0.05254	0.00475	0.16816	0.01481	0.02321	0.00049	309.0	193.3	157.8	12.9	147.9	3.1	93.7
05	16	332	461	0.7	0.04929	0.00149	0.16769	0.00478	0.02467	0.0002	161.6	69.4	157.4	4.2	157.1	1.3	99.8
06	7	297	211	1.4	0.04709	0.00247	0.14188	0.00721	0.02185	0.00027	53.6	121.1	134.7	6.4	139.3	1.7	96.6
07	3	78	78	1.0	0.04813	0.00316	0.15808	0.01012	0.02382	0.00034	105.5	148.4	149.0	8.9	151.8	2.2	98.1
08	19	456	618	0.7	0.05029	0.00132	0.15065	0.00367	0.02173	0.00016	208.4	59.9	142.5	3.2	138.6	1.0	97.3
09	2	44	53	0.8	0.04936	0.00657	0.16343	0.02135	0.02401	0.00064	165.0	284.2	153.7	18.6	153.0	4.0	99.5
10	3	54	59	0.9	0.04811	0.00507	0.14056	0.01451	0.02119	0.00046	104.7	231.8	133.5	12.9	135.2	2.9	98.7
11	18	200	539	0.4	0.04872	0.00116	0.17022	0.00369	0.02534	0.00018	134.5	54.8	159.6	3.2	161.3	1.1	98.9
12	2	53	48	1.1	0.04721	0.00451	0.15173	0.01421	0.02331	0.00044	59.2	213.5	143.4	12.5	148.5	2.8	96.4
13	4	138	110	1.2	0.04962	0.00322	0.14491	0.00917	0.02118	0.00028	177.4	144.5	137.4	8.1	135.1	1.8	98.3
14	3	141	90	1.6	0.0507	0.0047	0.15188	0.01382	0.02173	0.0004	227.2	201.1	143.6	12.2	138.6	2.5	96.5
15	2	50	56	0.9	0.04977	0.00427	0.15919	0.01336	0.0232	0.00041	184.1	188.3	150.0	11.7	147.8	2.6	98.5
16	5	176	136	1.3	0.05014	0.0027	0.15201	0.00794	0.02199	0.00027	201.4	120.4	143.7	7.0	140.2	1.7	97.6
17	11	292	331	0.9	0.04743	0.00161	0.14799	0.00477	0.02263	0.0002	70.3	79.5	140.1	4.2	144.2	1.3	97.1
18	4	126	92	1.4	0.04987	0.00236	0.15328	0.007	0.02229	0.00025	189.0	106.6	144.8	6.2	142.1	1.6	98.1
19	5	164	127	1.3	0.04897	0.00254	0.15459	0.00776	0.02289	0.00028	146.6	117.5	146.0	6.8	145.9	1.8	99.9
20	2	64	66	1.0	0.05041	0.00398	0.15632	0.01207	0.02249	0.00037	214.1	173.4	147.5	10.6	143.4	2.3	97.2
22	2	57	58	1.0	0.04956	0.00523	0.15403	0.0159	0.02254	0.00051	174.2	229.3	145.5	14.0	143.7	3.2	98.8
23	3	117	85	1.4	0.05423	0.00357	0.16425	0.0105	0.02197	0.00033	380.5	141.5	154.4	9.2	140.1	2.1	90.7
NMGZLN006																	
01	7	220	217	1.0	0.04972	0.00281	0.13493	0.00739	0.01968	0.00026	181.7	126.8	128.5	6.6	125.6	1.7	97.7
03	43	627	831	0.8	0.05504	0.00115	0.28065	0.00521	0.03697	0.00025	413.8	45.3	251.2	4.1	234.0	1.6	93.2
04	14	263	550	0.5	0.04614	0.00141	0.1191	0.00342	0.01872	0.00015	4.7	71.2	114.3	3.1	119.5	0.9	95.5
06	18	328	319	1.0	0.05368	0.00134	0.28151	0.00644	0.03803	0.00028	357.4	55.4	251.9	5.1	240.6	1.8	95.5
07	31	440	553	0.8	0.05342	0.00106	0.28398	0.00496	0.03855	0.00025	346.5	44.3	253.8	3.9	243.8	1.6	96.1
08	12	277	300	0.9	0.04965	0.00149	0.17699	0.00498	0.02585	0.00021	178.6	68.4	165.5	4.3	164.5	1.3	99.4
09	5	171	142	1.2	0.04892	0.00354	0.12277	0.00864	0.0182	0.00029	144.0	161.5	117.6	7.8	116.3	1.9	98.9
10	5	97	171	0.6	0.04801	0.00268	0.12436	0.00673	0.01878	0.00024	98.5	128.2	119.0	6.1	120.0	1.5	99.2
11	18	154	337	0.5	0.05358	0.00141	0.28889	0.00703	0.03909	0.0003	353.5	58.5	257.7	5.5	247.2	1.9	95.9
12	8	180	287	0.6	0.04823	0.00218	0.12802	0.00556	0.01925	0.00021	110.5	103.3	122.3	5.0	122.9	1.3	99.5
14	17	209	293	0.7	0.05309	0.00135	0.30347	0.00715	0.04145	0.00032	332.5	56.9	269.1	5.6	261.8	2.0	97.3
15	11	180	316	0.6	0.04983	0.00198	0.16996	0.00646	0.02473	0.00025	187.2	90.0	159.4	5.6	157.5	1.6	98.8
18	11	563	352	1.6	0.04718	0.00192	0.12404	0.00483	0.01907	0.00019	57.7	94.6	118.7	4.4	121.8	1.2	97.4
19	13	196	248	0.8	0.05392	0.00188	0.28588	0.00945	0.03845	0.00037	367.5	76.5	255.3	7.5	243.2	2.3	95.3
21	30	307	553	0.6	0.05079	0.001	0.28416	0.00496	0.04057	0.00027	231.4	44.9	254.0	3.9	256.4	1.6	99.1
22	19	198	648	0.3	0.0505	0.00153	0.15831	0.00452	0.02274	0.00019	217.8	68.9	149.2	4.0	144.9	1.2	97.1

.....continued on the next page

TABLE 2 (Continued)

Analyses					$^{207}Pb/^{206}Pb$		$^{207}Pb/^{235}U$		$^{206}Pb/^{238}U$		$^{207}Pb/^{206}Pb$		$^{207}Pb/^{235}U$		$^{206}Pb/^{238}U$		
	Pb	Th	U	Th/U	Ratio	1σ	Ratio	1σ	Ratio	1σ	Age	1σ	Age	1σ	Age	1σ	concordance
23	40	356	764	0.5	0.052	0.00091	0.284	0.00429	0.03961	0.00025	285.4	39.7	253.8	3.4	250.4	1.5	98.7
25	14	56	78	0.7	0.06514	0.00153	1.1881	0.02571	0.13229	0.00109	778.8	48.7	795.1	11.9	800.9	6.2	99.3
26	35	257	658	0.4	0.05215	0.00096	0.29208	0.00469	0.04062	0.00026	291.9	41.5	260.2	3.7	256.7	1.6	98.7
27	23	616	630	1.0	0.04858	0.00113	0.16142	0.00341	0.0241	0.00017	127.7	53.6	151.9	3.0	153.5	1.1	98.9
28	57	95	330	0.3	0.07025	0.00101	1.29923	0.01504	0.13415	0.00083	935.5	29.3	845.4	6.6	811.5	4.7	96.0
29	36	627	616	1.0	0.05442	0.00117	0.29348	0.00568	0.03912	0.00027	388.4	47.3	261.3	4.5	247.4	1.7	94.7
30	34	324	614	0.5	0.05565	0.00119	0.30924	0.00595	0.04031	0.00028	438.0	46.6	273.6	4.6	254.7	1.8	93.1
31	37	230	733	0.3	0.05231	0.00094	0.28719	0.00449	0.03982	0.00025	298.9	40.6	256.3	3.5	251.7	1.6	98.2
32	12	211	180	1.2	0.05386	0.00184	0.31167	0.01011	0.04198	0.0004	364.9	75.1	275.5	7.8	265.1	2.5	96.2
33	10	360	262	1.4	0.04965	0.00181	0.16316	0.00568	0.02384	0.00023	178.5	83.0	153.5	5.0	151.9	1.4	99.0
34	55	123	298	0.4	0.06494	0.00096	1.24853	0.01498	0.13947	0.00086	772.4	30.7	822.7	6.8	841.6	4.9	97.4
35	12	183	208	0.9	0.05022	0.00155	0.27276	0.00793	0.0394	0.00034	205.1	69.9	244.9	6.3	249.1	2.1	98.3
NMGZLN007																	
01	23	199	427	0.5	0.05183	0.0012	0.29425	0.00618	0.0412	0.0003	277.7	51.9	261.9	4.9	260.3	1.8	99.4
02	13	345	405	0.9	0.05	0.00198	0.16869	0.0064	0.02448	0.00025	194.8	89.7	158.3	5.6	155.9	1.6	98.5
03	11	165	228	0.7	0.05217	0.00171	0.26847	0.00833	0.03734	0.00033	293.0	73.1	241.5	6.7	236.3	2.1	97.8
04	11	415	281	1.5	0.05348	0.00237	0.18336	0.00779	0.02488	0.00028	349.0	96.9	170.9	6.7	158.4	1.8	92.7
05	5	69	95	0.7	0.05291	0.00357	0.26739	0.01754	0.03666	0.0006	324.8	145.8	240.6	14.1	232.1	3.7	96.5
06	18	352	317	1.1	0.05333	0.00163	0.29882	0.00858	0.04064	0.00035	343.0	67.7	265.5	6.7	256.8	2.2	96.7
07	18	131	383	0.3	0.05153	0.00134	0.28924	0.00693	0.04071	0.00031	264.7	58.4	258.0	5.5	257.2	1.9	99.7
08	16	47	97	0.5	0.06652	0.00176	1.23884	0.03045	0.13506	0.00121	822.8	54.2	818.4	13.8	816.7	6.9	99.8
09	29	237	604	0.4	0.05318	0.00113	0.29046	0.0055	0.03961	0.00027	336.4	47.3	258.9	4.3	250.4	1.7	96.7
10	11	261	334	0.8	0.05097	0.00181	0.16783	0.00566	0.02387	0.00022	239.7	79.8	157.5	4.9	152.1	1.4	96.6
11	9	86	155	0.6	0.05208	0.00217	0.29295	0.01169	0.04078	0.00043	289.0	92.2	260.9	9.2	257.7	2.7	98.8
12	5	69	101	0.7	0.05151	0.00255	0.27499	0.01312	0.0387	0.00047	263.9	109.5	246.7	10.5	244.8	2.9	99.2
13	15	240	292	0.8	0.05144	0.00157	0.26004	0.00746	0.03664	0.00031	260.7	68.6	234.7	6.0	232.0	1.9	98.8
14	5	195	137	1.4	0.05088	0.00283	0.16684	0.00899	0.02376	0.0003	235.4	123.4	156.7	7.8	151.4	1.9	96.6
15	4	49	72	0.7	0.05383	0.00305	0.28858	0.01584	0.03886	0.00053	363.7	122.4	257.4	12.5	245.7	3.3	95.5
16	4	64	83	0.8	0.04998	0.00284	0.26436	0.0146	0.03833	0.00049	194.2	127.0	238.2	11.7	242.5	3.1	98.2
17	11	240	345	0.7	0.05036	0.00193	0.16447	0.00601	0.02366	0.00023	211.8	86.5	154.6	5.2	150.8	1.4	97.5
18	9	134	162	0.8	0.05187	0.00207	0.27884	0.01062	0.03895	0.0004	279.8	88.5	249.7	8.4	246.3	2.5	98.6
19	18	367	388	0.9	0.05458	0.00191	0.24062	0.00797	0.03194	0.0003	395.0	75.9	218.9	6.5	202.7	1.9	92.6
20	5	144	185	0.8	0.05233	0.00347	0.131	0.00844	0.01814	0.00028	299.7	144.4	125.0	7.6	115.9	1.8	92.7
21	5	121	194	0.6	0.04995	0.00397	0.12535	0.00969	0.01818	0.00032	192.5	174.8	119.9	8.8	116.2	2.1	96.9
22	6	80	110	0.7	0.05241	0.0024	0.28004	0.01233	0.03871	0.00044	303.5	101.0	250.7	9.8	244.8	2.7	97.6
23	4	58	80	0.7	0.05226	0.00348	0.25861	0.01675	0.03585	0.00056	296.7	145.0	233.5	13.5	227.1	3.5	97.3
24	5	60	94	0.6	0.05334	0.00414	0.2843	0.02147	0.03861	0.00072	343.3	166.3	254.1	17.0	244.2	4.5	96.1
25	9	112	176	0.6	0.05401	0.00213	0.29159	0.01097	0.03911	0.0004	371.3	86.1	259.8	8.6	247.3	2.5	95.2
26	49	160	284	0.6	0.06921	0.00115	1.24	0.0172	0.12978	0.00084	904.9	33.9	818.9	7.8	786.6	4.8	96.1

Analysers are Agilent 7500, laser is 32μm and error is 1 σ. Calculated by Glitter.

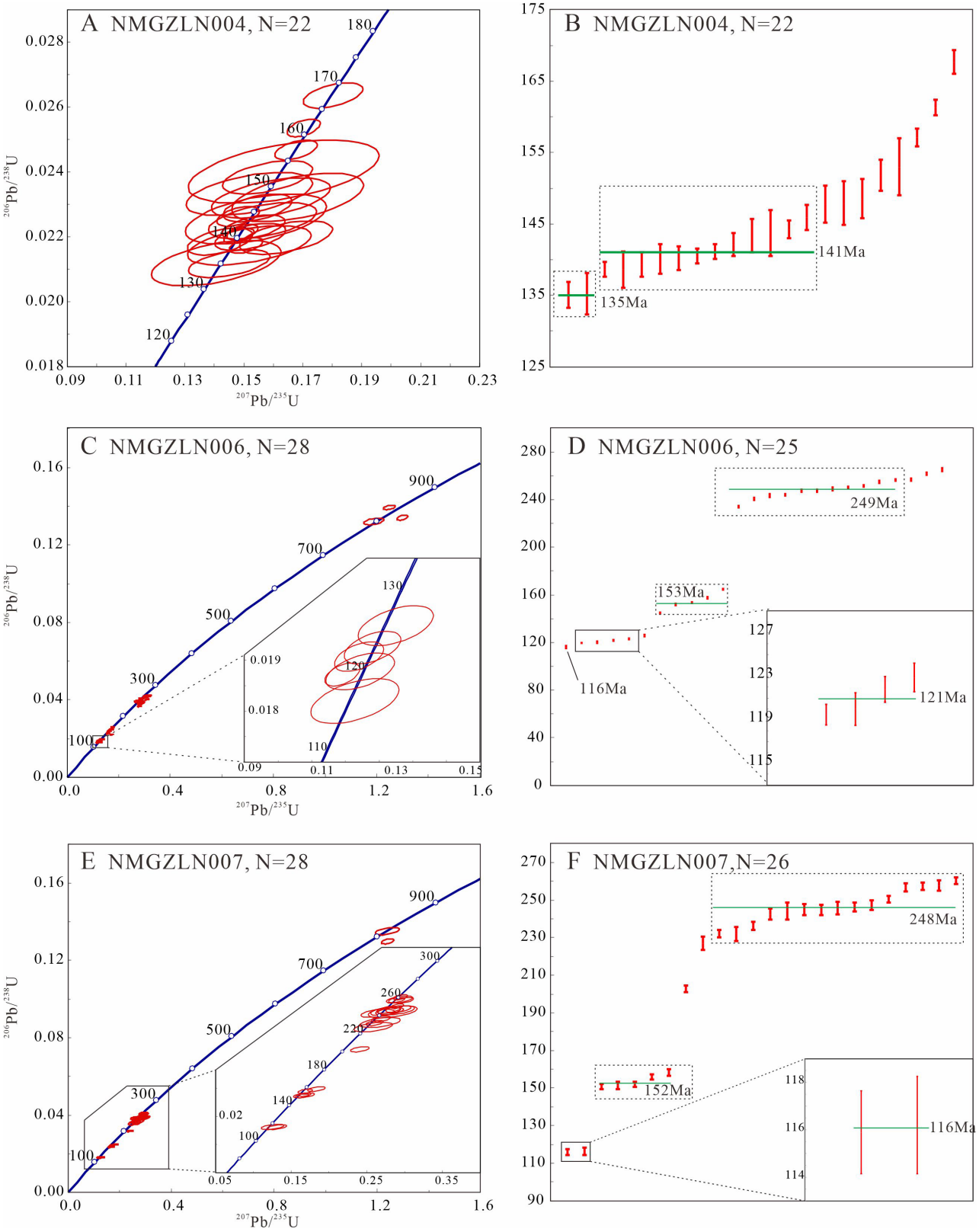

FIGURE 7. Age plots for samples from Damoguaihe Formation of Zhalainuoer Coal Mine. **A**, **C**, **E**, Zircon U-Pb concordia age plots for these samples. **B**, **D**, **F**, Weighted mean age plots for these samples. Youngest ages were amplified in insets. Locations of samples are marked in FIGURE 3. Green line represents weighted mean age of a group of analyses marked by rectangles.

origin. Data points that were scattered or exhibited lower concord (typically < 90%) were excluded when plotting the concordia and weighted mean age plots.

Twenty-three grains from the sample NMGZLN004 were analyzed and one analysis was rejected due to discordant. The ages of the remaining grains range

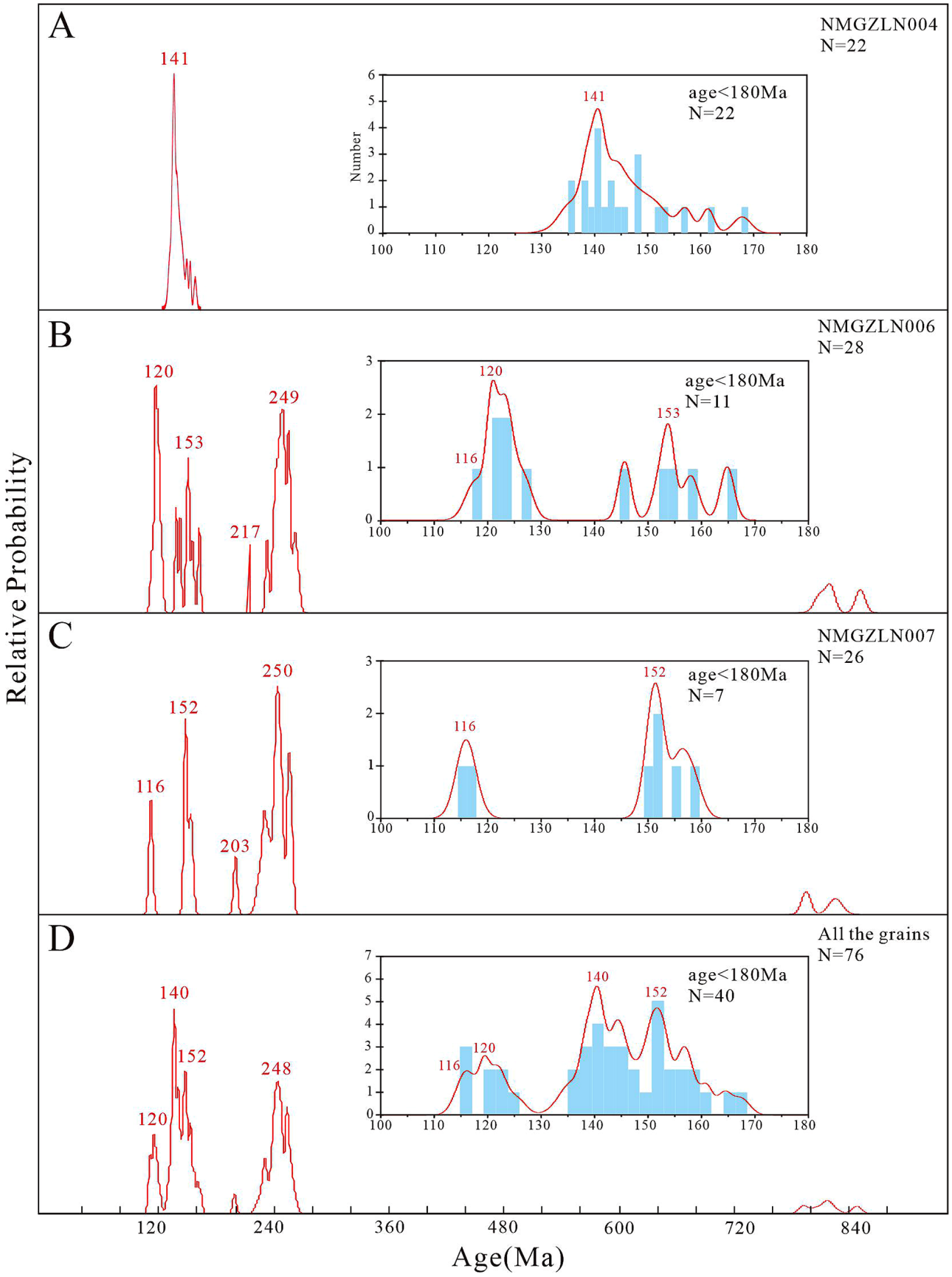

FIGURE 8. Age-probability plots of samples from Damoguahe Formation in Hailar Basin. Partial enlarged drawings (age < 180 Ma) were shown in insets.

from 135 to 168 Ma. Among them, the two youngest analyses are *ca*. 135 Ma, and a group of twelve relatively concentrated analyses yield a weighted mean age of 141 ± 1 Ma. The other eight points scatter in the age span of 148–168 Ma (Figs. 7A, B). The detrital zircon age spectrum is characterized by a significant age peak (*ca*. 141 Ma) and a dispersed tail ranging from 152–168 Ma (Fig. 8A).

Thirty-five grains from the sample NMGZLN006 were analyzed and five analyses were rejected due to discordant. Apart from three old Neoproterozoic ages (801, 842 and 812 Ma), other ages range from 116–265 Ma, forming two significant clusters at *ca*. 120 and 249 Ma, as well as a less apparent age peak of 153 Ma (Fig. 8B). The youngest age is 116 Ma (Fig. 7D).

Twenty-six grains were analyzed for the sample NMGZLN007. Except for two Neoproterozoic ages (787 and 817 Ma), the remaining ages range from 116–260 Ma., exhibiting two prominent clusters at *ca*. 152 and 250 Ma (Fig. 8C). Two zircon grains yielded the youngest weighted mean age of 116 Ma (Fig. 7F).

Detrital zircon spectrum of all the grains shows four age clusters (Fig. 8D) of *ca*. 120, 140, 152 and 248 Ma, and several sporadic Neoproterozoic ages.

FT-IR analysis

The obtained spectra (Fig. 6) of the two analyzed amber samples are comparable to the spectrum of amber obtained by Azar *et al*. (2019) from the same locality. The spectra could be divided into two areas: transmittance bands between 3700–1350 cm^{-1} are almost shared by all types of amber; transmittance bands between 1350–400 cm^{-1} are the fingerprint area. Transmittance strong and broad peak at the wavelength 3449 (in A) and 3435 (in B) cm^{-1} corresponds to O-H stretching in alcohol and/or carboxylic acid. Transmittance peak at 2967 (in B) cm^{-1} corresponds to N-H stretching in amine salt. Transmittance peak at the wavelength 2926 cm^{-1} in both spectra corresponds to C-H stretching in CH, CH_2 and CH_3. Transmittance peak at the wavelengths 2852 (in A) and 2853 (in B) cm^{-1} corresponds to C-H stretching in CH, CH_2 and CH_3. Transmittance peak at the wavelength 1695 cm^{-1} (in both spectra) corresponds to C=O stretching in carboxylic acids. Transmittance peaks at the wavelength 1641 (in A and B) cm^{-1} corresponds to C=C stretching in conjugated alkene. Transmittance peak at the wavelength 1467 cm^{-1} (in both spectra) corresponds to C-H bending in CH_2 and CH_3 of alkyl groupings. Transmittance peak at the wavelength 1378 (in A) and 1377 (in B) cm^{-1} respectively corresponds to C-H bending in CH_3 of alkyl groupings. Transmittance peak at the wavelengths 1177 (in A) and 1178 (in B) cm^{-1} corresponds to C-O stretching in carboxylic acids and esters. Transmittance peak at the wavelength 1032 (in both spectra) cm^{-1} corresponds to S=O stretching in sulfoxide. The transmittance peak at the wavelength 977 (in both spectra) cm^{-1} corresponds to C-H bending in CH_2 of cycloalkane. All the functional groups detected indicate the large dominance of the aliphatic chains in the chemical constitution of the studied amber. It is noteworthy to state that infrared analyses have long been used in amber characterization; however, used only by itself, they cannot be necessarily precise in correctly ascertaining the botanical origin of the amber.

Discussion

Age of the amber in the Damoguaihe Formation

As mentioned above, the Damoguaihe Formation was generally assigned to be Valanginian–early Albian based on different fossil assemblages (Table 1). It seems like the ages based on spore assemblages are older than those of other fossil assemblages. The youngest detrital zircon grains may approximate the time of sediment accumulation, especially when there were syn-sedimentary magmatic activities (Cawood *et al*., 2012). The Youngest age in our results is 116 Ma, indicating that the upper part of the Damoguaihe Formation is younger than this age. The Ganhe Formation, predominated by a set of basalt, overlies or contact with the Damoguaihe formations resembling crossed fingers (IBGMR, 1996). This observation suggests that the upper part of the Damoguaihe Formation is simultaneous or older than the Ganhe Formation. The age of the Ganhe Formation has been dated as 120–113 Ma (Yang *et al*., 2022). Therefore, the upper part of Damoguaihe is constrained from 116 to 113 Ma, belonging to the late Aptian. In other words, based on our findings, we can conclude that amber found in the Damoguaihe Formation dates to the late Aptian period.

Age of the amber in the Yimin Formation

The Yimin Formation has been determined to be Barremian to Albian according to the fossil assemblage. Currently, the amber has been discovered in two layers within this unit: the Zhalainuoer Coal Mine and the lowest part in the Yimin Coal Mine, with respective dates of 111.7 ± 2.2 Ma and 130.9 ± 2.8 Ma determined by detrital zircon U-Pb ages (Li *et al*., 2023). The former is supported by our findings, while the latter contradicts evidence from biostratigraphy and acquired isotopic ages (Ji *et al*., 2019; this study).

The youngest detrital zircon ages could constrain the maximum depositional ages of stratigraphic units (Dickinson & Gehrels, 2009), however, it is important to consider potential time lags between these ages, which may be influenced by a lot of factors, such as sample

counts, sediment provenance, and the frequency of regional tectono-thermal events. For instance, signals of the latest tectono-thermal event may be disappeared in the age spectrum due to a lack of corresponding sediment contribution or a small number of analysis spots. Our dating suggests that the upper part of the Damoguaihe Formation is younger than 116 Ma, thus the overlying Yimin Formation should be late Aptian to Albian (mainly Albian).

Peak ages in the age spectrum

The peaks in the detrital zircon age spectrum are responses to regional magmatic activities and/or metamorphic events (Cawood *et al*., 2012). The Zhalainuoer Coal Mine is located in the Northwestern part of the Hulunhu Depression of the Hailar Basin (Figs. 2C, D), with its potential sedimentary sources including slopes to the west, uplift in the faulted basin, and/or volcanic ash from the syn-sedimentary volcanic eruptions (A *et al*., 2013).

The sample NGMZLN004 exhibits an age range of 135–168 Ma, with a peak age of 141 Ma. This age distribution suggests that the deposits mainly originate from the Tongbomiao Formation, which was deposited during the period of 142–137 Ma (Ji *et al*., 2019). Considering that the Middle to Late Jurassic Wanbao (165–162 Ma; Zhang *et al*., 2018) and Tamulangou formations (157–148 Ma; Ji *et al*., 2019) could be the sediment source of the Tongbomiao Formation, the Tongbomiao Formation can yield age signals as old as those from the Wanbao and Tamulangou formations.

Compared to sample NGMZLN004, the detrital zircon age spectra of the other two samples show several important features as follows:

1) The cluster at *ca*. 140 Ma exhibited a gradual disappearance, with two ages (*ca*. 141 and 145 Ma) preserved in the sample NGMZLN006, while completely absent in the sample NGMZLN007. Concurrently, the signals at *ca*. 152–153 Ma are increasing. Both observations indicate a gradual shift in provenance area from the overlying Tongbomiao Formation to the underlying Wanbao and Tamulangou formations due to continuous denudation.

2) The peak age of 250 Ma was observed in both samples NGMZLN006 and NGMZLN007. In the Manzhouli area, to the west of the Hailar Basin, some latest Permian granites (*ca*. 250 Ma; Meng *et al*., 2011; Gou *et al*., 2013) are exposed. These granites likely underwent uplifting and denudation, which could provide detrital materials during the deposition of these layers

3) The peak age of 120 Ma was observed in the sample NGMZLN006, but subsequently disappeared in sample NGMZLN007, with only one age of 116 Ma present. This indicates that the signal source of *ca*. 120 Ma is not stable, most likely due to the deposition of the falling ash.

4) A small proportion of ages at *ca*. 800 Ma were identified in both samples NGMZLN006 and NGMZLN007. These ages should be contributed to the basement of the Erguna massif. The Paleozoic–Mesozoic magmatic activities in the Erguna massif may have carried inherited zircons with Neoproterozoic ages. In contrast, the basement of the Xing'an block lacks such old-age signatures (Xu *et al*., 2013), indicating a predominant provenance from the Erguna block in the northwest.

The aforementioned evidence suggests that the primary source of sediment is the western slope of the Hulunhu Depression, with a minor contribution from ash deposition resulting from syn-sedimentary volcanic activities.

Conclusion

Our results suggest that the upper part of the Damoguaihe Formation in the Hailar Basin, where the tiny amber piece was found (Azar *et al.*, 2019), is slightly later than 116 Ma (late Aptian), consistent with previous biostratigraphy and isotopic chronology. This further confirms that the Buir Lake ambers are from the upper Lower Cretaceous Daomoguaihe Formation and Yimin Formation, dating to Aptian–Albian.

The age spectrum of the clastic rocks indicates that the primary source of sediment is the western slope of the Hulunhu Depression, with a minor contribution from ash deposition resulting from syn-sedimentary volcanic activities.

Acknowledgment

We thank two anonymous reviewers for their valuable comments on an earlier version of this paper. This work was supported by the National Natural Science Foundation of China (41925008 and 42288201).

Reference

A, M.N., Zhang, F.Q. Yang, S.F., Chen, H.L., Batt, G.E., Sun, M.D., Meng, Q.A., Zhu, D.F., Cao, R.C. & Li, J.S. (2013) Early Cretaceous provenance change in the southern Hailar Basin, northeastern China and its implication for basin evolution. *Cretaceous Research*, 40, 21–42. https://doi.org/10.1016/j.cretres.2012.05.005

Azar. D., Maksoud, S., Cai, C.Y. & Huang, D.Y. (2019) A new amber outcrop from the Lower Cretaceous of northeastern China. *Palaeoentomology*, 2 (4), 345–349. https://doi.org/10.11646/palaeoentomology.2.4.8

Bray, P.S. & Anderson, K.B. (2009) Identification of Carboniferous (320 million years old) class Ic amber. *Science*, 326, 132–134.
https://doi. org/10.1126/science.1177539

Cawood, P.A., Hawkesworth, C.J. & Dhuime, B. (2012) Detrital zircon record and tectonic setting. *Geology*, 40 (10), 875–878.
https://doi.org/10.1130/G32945.1

Chen, C.Y., Gao, Y.F., Wu, H.B., Qu, X.J., Liu, Z.W., Bai, X.F. & Wang, P.J. (2016) Zircon U-Pb chronology of volcanic rocks in the Hailaer Basin, NE China and its geological implications. *Earth Science*, 41 (8), 1259–1274. [In Chinese with English abstract]

Delclòs, X., Peñalver, E., Barrón, E., Peris, D., Grimaldi, D.A., Holz, M., Labandeira, C.C., Saupe, E.E., Scotese, C.R., Solórzano-Kraemer, M.M. & Álvarez-Parra, S. (2023) Amber and the Cretaceous resinous interval. *Earth-Science Reviews*, 243, 104486.
https://doi.org/10.1016/j.earscirev.2023.104486

Dickinson, W.R. & Gehrels, G.E. (2009) Use of U–Pb ages of detrital zircons to infer maximum depositional ages of strata: A test against a Colorado Plateau Mesozoic database. *Earth and Planetary Science Letters*, 288, 115–125.
https://doi.org/10.1016/j.epsl.2009.09.013

Gou, J., Sun, D.Y., Ren, Y.S., Liu, Y.J., Zhang, S.Y., Fu, C.L., Wang, T.H., Wu, P.F. & Liu, X.M. (2013) Petrogenesis and geodynamic setting of Neoproterozoic and Late Paleozoic magmatism in the Manzhouli—Erguna area of Inner Mongolia, China: Geochronological, geochemical and Hf isotopic evidence. *Journal of Asian Earth Sciences*, 67–68, 114–137.
https://doi.org/10.1016/j.jseaes.2013.02.016.

Han, G., Cao, Y., Zhang, W.J. Wang, J.Y., Xue, Y.F. & Bao, L. (2019) Stratigraphy and sporo-pollen assemblages of well Bei 32 from the Nantun Formation in the Hailar Basin, Inner Mongolia. *Geological Bulletin of China*, 2019, 38 (6), 916–921.

Huang, Q.H., Zhao, L.S., Lu, Z.W., Dang, Y.M., Wang, L.Q. & Kong, H. (2006) Sporopollen fossil of the Damoguaihe Formation and its age in Hailaer Basin, Inner Mongolia. *Geological Science and Technology Information*, 25 (1), 19–26. [In Chinese with English abstract]

Inner Mongolia Bureau of Geological and Mineral Survey (IBGMR) (1996) Strata of the Inner Mongolia Province. *China University of Geosciences Press*, Wuhan, 354 pp. [In Chinese]

Ji, Z., Wan, C.B., Meng, Q.A., Zhu, D.F., Ge, W.C., Zhang, Y.L., Yang, H., Dong, Y. & Jing, Y. (2019) Chronostratigraphic framework of late Mesozoic terrestrial strata in the Hailar–Tamtsag Basin, Northeast China, and its geodynamic implication. *Geological Journal*, 55 (7), 5197–5215.
https://doi.org/10.1002/gj.3731

Li, C.B., Wan, C.B., Qiao, X.Y., Shan, X.L., Wang, L.Y. Shao, H.J., Chi, H.Y. & Liu, T.Y. (2007) Pollen and spore assemblages of the Yimin Formation of Haican-1 Well, Hailaer Basin and their stratigraphic significance. *Journal of Stratigraphy*, 31 (1), 23–34. [In Chinese with English abstract]

Li, P.P., Ge, W.C. & Zhang, Y.L. (2010) Division of volcanic strata in the northwestern part of Hailar basin: evidence from zircon U-Pb dating. *Acta Petrologica Sinica*, 26 (8), 2482–2494.

Li, Y.L, Zheng, D.R., Sha, J.G., Zhang, H.C., Denyszyn, S. & Zhang, S.C. (2023) Lower Cretaceous Hailar amber: the oldest-known amber from China. *Cretaceous Research*, 145, 105472.
https://doi.org/10.1016/j.cretres.2022.105472

Ludwig, K.R. (2003) User's manual for Isoplot 3.0. *A geochronological toolkit for Microsoft Excel*. Berkeley Geochronology Centre, Berkeley, California, Special Publication, 4a, 1–70.

Meng, E., Xu, W.L., Yang, D.B., Qiu, K.F., Li, C.H. & Zhu, H.T. (2011) Zircon U-Pb chronology, geochemistry of Mesozoic volcanic rocks from the Zhalainuoer basin in Manzhouli area, and its tectonic implications. *Acta Petrologica Sinica*, 27 (4), 1209–1226. [In Chinese with English abstract]

Meng, Q.A, Wan, C.B., Qiao, X.Y., Sun, Y.W., Shan, X.L., Xu, Y.B., Ren, Y.G. & Zhao, C.B. (2003) Palynological assemblages from the Damoguaihe Formation in the Hailar Basin, Inner Mongolia. *Journal of Stratigraphy*, 27 (3), 173–184. [In Chinese with English abstract]

Meng, Q.A, Wan, C.B., Zhu, D.F., Zhang, Y.L. Ge, W.C. & Wu, F.Y. (2013) Age assignment and geological significance of the "Budate Group" in the Hailar Basin. *Science China: Earth Sciences*, 56, 970–979.
https://doi.org/10.1007/s11430-013-4614-5

Ni, Z.J., Song, X.B., Azar, D., Wwang, Z.X., Cai, C.Y., Xuan, Q., Maksoud, S., Lian, X.N. & Huang, D.Y. (2023) Discovery of Late Cretaceous amber from Guangzhou, South China. *Palaeoentomology*, 6 (4), 329–332.
https://doi.org/10.11646/palaeoentomology.6.4.3

Pu, R.G. & Wu, H.Z. (1985) The palynological assemblages of the Hingganling and Zhalainuoer in Hinggan Ling Region, Northeast China and their stratigraphical significance. *Bull. Shenyang, Inst. Geol. Min. Res., Chinese Acad. Geol. Sci*, 11, 47–113. [In Chinese with English abstract]

Roghi, G., Gianolla, P., Kustatscher, E., Schmidt, A.R. & Seyfullah, L. (2022) An exceptionally preserved Terrestrial record of LIP effects on plants in the Carnian (Upper Triassic) amber-bearing section of the Dolomites, Italy. *Frontiers in Earth Science*, 10, 900586.
https://doi.org/10.3389/feart.2022.900586

Şengör, A.M.C., Natal'in, B.A. & Burtman, V.S. (1993) Evolution of the altaid tectonic collage and Palaeozoic crustal growth in Eurasia. *Nature*, 364, 299–307.
https://doi.org/10.1038/364299a0

Shi, G.L., Dutta, S., Paul, S. Wang, B. & Jacques, F.M.B. (2014) Terpenoid compositions and botanical origins of Late Cretaceous and Miocene amber from China. *PLoS ONE*, 9 (10), 0111303.
https://doi.org/10.1371/journal.pone.0111303

Stilwell, J. D., Langendam, A., Mays, C., Sutherland, L.J.M., Arillo, A., Bickel, D.J., Silva, W.T.D., Pentland, A.H., Roghi, G., Price, G.D., Cantrill, D.J., Quinney, A. & Penalver, E. (2020) Amber from the Triassic to Paleogene of Australia and New Zealand as exceptional Preservation of poorly known terrestrial ecosystems. *Scientific Reports*, 10 (1), 5703. https://doi.org/10.1038/s41598-020-62252-z

Tian, Y.K., Chu, D.L., Cao, Y., Corso, J.D., Roghi, G., Song, H.J., Tian, L., Liu, C.Y., He, X., Miao, X., Zhang, S.Y., Shu, W.C. & Tong, J.N. (2024) Anisian (Middle Triassic) amber from Qingyan section, Guizhou Province and its significance. *Earth Science*, 49 (4), 1515–1523. [In Chinese with English abstract] https://doi.org/10.3799/dqkx.2023.182

Wan, C.B. (2006) *Cretaceous palynological flora in Hailar Basin*. PhD Thesis of Jilin University, Changchun, 209 pp. [In Chinese with English abstract]

Wang, L.Y., Wan, C.B. & Sun, Y.W. (2014) A spore-pollen assemblage from the Damoguaihe Formation in the Tamutsag Basin, Mongolia and its geological implication. *Acta Geologica Sinica*, 88 (1), 46–61. https://doi.org/10.1111/1755-6724.12182

Wang, Y.Q., Sha, J.G., Pan, Y.H., Zhang, X.L. & Rao, X. (2012) Non-marine Cretaceous ostracod assemblages in China: a preliminary review. *Journal of Stratigraphy*, 36, 289–299.

Wilde, S.A. & Zhou, J.B. (2015) The late Paleozoic to Mesozoic evolution of the eastern margin of the Central Asian Orogenic Belt in China. *Journal of Asian Earth Sciences*, 113, 909–921. https://doi.org/10.1016/j.jseaes.2015.05.005

Windley, B.F., Alexeiev, D., Xiao, W.J., Kr öner, A. & Badarch, G. (2007) Tectonic models for accretion of the Central Asian Orogenic Belt. *Journal of the Geological Society, London*, 164, 31–47. https://doi.org/10.1144/0016-76492006-022

Wu, H., Huang, Q., Dang, Y., Kong, H. & Wang, L. (2006) Achievements in the study on Cretaceous biostratigraphy of the Hailar Basin, Inner Mongolia. *Acta Palaeontologica Sinica*, 45, 283–291. [In Chinese with English abstract]

Xu, W.L., Pei, F.P., Wang, F., Meng, E., Ji, W.Q., Yang, D.B. & Wang, W. (2013) Spatial-temporal relationships of Mesozoic volcanic rocks in NE China: Constraints on tectonic overprinting and transformations between multiple tectonic regimes. *Journal of Asian Earth Sciences*, 74, 167–193. https://doi.org/10.1016/j.jseaes.2013.04.003

Xue, Y.F. (2017) Sporopollen assemblages and their geological significances for Yimin Formation in Chargannuoer Sag of Hailer Basin. *Petroleum Geology and Oilfield Development in Daqing*, 36 (2), 52–59. [In Chinese with English abstract]

Xue, Y.F. & Wang, L.Y. (2010) Jalai Nur Group sporopollen assemblages in Qagan Nur Depression, Hailar Basin. *Coal Geology of China*, 22 (1), 6–9. [In Chinese with English abstract]

Yang, Y.J., Yang, X.P., Jiang, B., Wang, Y. & Pang, X.J. (2022) Spatio-temporal distribution of Mesozoic volcanic strata in the Great Xing'an Range: response to the subduction of the Mongol-Okhotsk Ocean and Paleo-Pacific Ocean. *Earth Science Frontiers*, 29 (2), 115–131. [In Chinese with English abstract]

Zhang, Y. Wu, X., Zhang, C., Guo, W, Yang, Y. & Sun, G. (2018) New evidence for dating of the Middle Jurassic Wanbao Formation in the Longjiang Basin, western margin of Heilongjiang Province. *Earth Science Frontiers*, 25 (1), 182–196. [In Chinese with English abstract]

Zhao, L., Gao, F.H., Zhang, Y.L., Xu, H.M. & Zhang, L.Y. (2015) Zircon U-Pb chronology and its geological implications of Mesozoic volcanic rocks from the Hailaer basin. *Acta Petrologica Sinica*, 29 (3), 864–874. [In Chinese with English abstract]

Zhong, B.H. (2003) Amber resource of China. *Journal of Gems & Gemmology*, 5 (2), 33. [In Chinese with English abstract]